



UNIVERSITY OF LEEDS

This is a repository copy of *A statistical approach to the inclusion of electrode contact impedance uncertainty in electrical tomography reconstruction*.

White Rose Research Online URL for this paper:
<http://eprints.whiterose.ac.uk/122974/>

Version: Accepted Version

Article:

Aykroyd, RG orcid.org/0000-0003-3700-0816 (2018) A statistical approach to the inclusion of electrode contact impedance uncertainty in electrical tomography reconstruction. *International Journal of Tomography and Simulation*, 31 (1). pp. 56-67. ISSN 2319-3336

© 2018 International Journal of Tomography & Simulation. This is an author produced version of a paper published in *International Journal of Tomography & Simulation*. Uploaded with permission from the publisher.

Reuse

Items deposited in White Rose Research Online are protected by copyright, with all rights reserved unless indicated otherwise. They may be downloaded and/or printed for private study, or other acts as permitted by national copyright laws. The publisher or other rights holders may allow further reproduction and re-use of the full text version. This is indicated by the licence information on the White Rose Research Online record for the item.

Takedown

If you consider content in White Rose Research Online to be in breach of UK law, please notify us by emailing eprints@whiterose.ac.uk including the URL of the record and the reason for the withdrawal request.



eprints@whiterose.ac.uk
<https://eprints.whiterose.ac.uk/>

A statistical approach to the inclusion of electrode contact impedance uncertainty in electrical tomography reconstruction

Robert G. Aykroyd*
University of Leeds

ABSTRACT

Electrical tomography is a visualisation tool used for industrial process monitoring. The complete electrode model relates an unknown conductivity field with the measurements but also involves unknown electrode contact impedances. Here, a real data analysis shows that the contact impedances vary spatially and with time. Then, the main reconstruction process is repeated using contact impedance values drawn at random from a fitted contact impedance distribution, and a model average calculated as the final reconstruction. This additional source of variation can then be appropriately accounted for thereby preventing overly optimistic assumption in subsequent decision making.

Keywords: Bayesian model averaging; electrical impedance tomography; finite-element method; temporal variability; uncertainty quantification.

1 Introduction

Electrical tomographic techniques, where a section through an object is imaged using voltage measurements taken outside the object, are well known, especially for industrial and medical applications. Electrodes are attached to the boundary of the object, then currents are applied and measurements of voltage are recorded at the electrodes. The relationship between resistivity and voltages is non-linear and to find the resistivity for given voltages is an inverse problem requiring regularization in order to ensure stability and reliability (Kaipio, Kolehmainen, Vauhkonen and Somersalo, 1999). If the contents of the domain are known, then boundary voltages can be calculated through the solution of Maxwell's equations and corresponding boundary conditions (Somersalo, Cheney and Isaacson, 1992) for electromagnetism. Such inverse problems cannot be solved analytically and instead require substantial numerical effort. The most common

*Contact details: School of Mathematics, University of Leeds, Leeds, LS2 9JT, UK, e-mail: r.g.aykroyd@leeds.ac.uk

approach is to divide-up the region of interest into a grid of pixels, whose values require estimation. In practice this is done numerically, and often using the finite element method (Vauhkonen, Lionheart, Heikkinen, Vauhkonen and Kaipio, 2001; Lionheart, 2004). This is the direct problem or forward solution. It is well posed and voltages can be obtained at least to the accuracy of measurements. The resulting image reconstruction usually becomes an ill-conditioned and ill-posed inverse problem. It has been shown, see for example (Heikkinen, Vilhunen, West and Vauhkonen, 2002) and (Paulson, Breckon and Pidcock, 1992), that it is important to model contact impedance. Contact impedances which can be very large for several industrial applications (Vilhunen, Kaipio, Vauhkonen, Savolainen and Vauhkonen, 2002; Heikkinen et al., 2002). The contact impedance is a nuisance parameter but has considerable influence. For this reason contact impedance needs to be modelled with great care. In the work presented here, a novel approach is taken to determine a plausible range for the contact impedances from the data obtained in a calibration step of the experiment and its inclusion in the reconstruction process.

This paper is organized as follows. Background to the complete electrode mode for EIT is described in section 2 along with details of statistical modelling. The proposed technique for quantifying the effects of the electrode contact impedance on reconstruction reliability is given in Section 3. Section 4 gives information about the data and the results of its analysis. The final discussion appears in Section 5.

2 Electrical tomography model

Suppose that the cross section of the circular tank is partitioned into n triangular pixels, labelled by the integers $1, 2, \dots, n$. In the direct problem, the resistivity ρ_i of each pixel ($i = 1, 2, \dots, n$) is specified. An assumption here is that resistivity ρ_i is constant across pixel i . The electric field potential, ϕ , is required at points of the domain boundary from which potential differences, voltages, can be calculated.

Within the domain Ω Maxwell's equations can be condensed to the condition

$$\nabla \cdot (\sigma \nabla \phi) = 0, \quad (2.1)$$

for the conductivity vector $\sigma \in (\mathbb{R}^+)^n$ with $\sigma = 1/\rho$. The boundary of the domain ($\partial\Omega$) will comprise electrodes E_k ($k = 1, 2, \dots, K$), and edges where the boundary is insulating. Current pattern $\underline{I} = \{I_1, I_2, \dots, I_K\}$, with I_k the amplitude of the current injected through the electrode E_k , is applied to the electrodes with appropriate boundary conditions on the electrodes.

Data will be collected using several different current patterns. In our experiments a widely used 'reference protocol' is chosen where the current patterns consists of injecting current between the reference electrode and each of the other electrodes in turn, hence producing $K - 1$ current patterns (for details see West *et al.* 2001) and leading to $m = (K - 1)^2$ measured voltages. Note

that this protocol provides most information about the image nearer to the site of the reference electrode. Although this is a widely used protocol, alternatives such as trigonometric or adaptive current patterns (Isaacson 1986) may lead to better reconstruction.

This modelling leads to the boundary conditions on the electrodes

$$\left. \begin{aligned} \left(\phi + z_k \sigma \frac{\partial \phi}{\partial \mathbf{n}} \right) \Big|_{E_k} &= U_k, \quad \int_{E_k} \sigma \frac{\partial \phi}{\partial \mathbf{n}} dS = I_k, \quad k = 1, 2, \dots, K, \\ \sigma \frac{\partial \phi}{\partial \mathbf{n}} \Big|_{\partial \Omega \setminus \bigcup_{k=1}^K E_k} &= 0, \end{aligned} \right\} \quad (2.2)$$

whilst on the insulating boundaries between electrodes

where $\mathbf{z} = \{z_1, z_2, \dots, z_K\}$ are the contact impedances on the electrodes, U_k denotes the potential on the k^{th} electrode E_k , and \mathbf{n} is the outward unit normal of the boundary. It is common to assume a single contact impedance for all electrodes, that is $\mathbf{z} = z_0 \{1, 1, \dots, 1\}$, however, here estimation of the individual electrode contact impedances is considered.

The pixellization of the domain is determined by both physical and imaging considerations. The aim is to use these data to reconstruct the unknown resistivity pattern at all the time points, that is to estimate $\boldsymbol{\rho} = \{\rho_1, \rho_2, \dots, \rho_m\}$. Physically we require the boundary pixels to have an outer edge as long as the width of our electrodes, and the sum of edge length between the electrodes to reflect the actual spacing of the electrodes. For useful imaging a moderately large number of pixels are needed so that small features will cover several pixels. For a known resistivity or conductivity distribution Equation (2.1) with boundary conditions Equation (2.2), can be solved for the electrical potential using the finite element method (Vauhkonen et al., 2001). This requires a finer mesh in order to deliver accurate solution, which can be most easily handled by subdivision of the pixellization. Here, all calculations are performed in Matlab using the EIDORS library (Polydorides and Lionheart, 2002).

The data are related to the resistivity through a measurement model

$$\mathbf{V} = \mathbf{V}^*(\boldsymbol{\rho}, \mathbf{z}) + \boldsymbol{\epsilon}, \quad (2.3)$$

where $\mathbf{V}^*(\boldsymbol{\rho}, \mathbf{z})$ are calculated from the forward model. This states that the measured voltages are equal to the theoretical values plus a, usually small, measurement error. It is assumed that the errors are independent and have common variance, which has been confirmed through extensive practical experience with the instrumentation. This leads to the likelihood: the conditional distribution of \mathbf{V} given $\boldsymbol{\rho}$ and \mathbf{z} , defined as $\mathbf{V} | \boldsymbol{\rho}, \mathbf{z} \sim N(\mathbf{V}^*(\boldsymbol{\rho}, \mathbf{z}), \sigma^2 I)$, with density function

$$f(\mathbf{V} | \boldsymbol{\rho}, \mathbf{z}) = \frac{1}{(2\pi\sigma^2)^{m/2}} \exp \left\{ -\frac{1}{2\sigma^2} \|\mathbf{V} - \mathbf{V}^*(\boldsymbol{\rho}, \mathbf{z})\|^2 \right\}, \quad (2.4)$$

where the 2-norm is used corresponding to a Gaussian distribution. The aim is then to reconstruct the unknown resistivity pattern, that is to estimate $\boldsymbol{\rho} = \{\rho_1, \rho_2, \dots, \rho_m\}$, given the data, $\mathbf{V} = \{V_1, V_2, \dots, V_n\}$, with the contact impedances $\mathbf{z} = \{z_1, z_2, \dots, z_K\}$ taken as unknown nuisance parameters. It is worth noting, that if it were assumed that the contact impedances were known then the left hand-side in Equation (2.4) would reduce to $f(\mathbf{V}|\boldsymbol{\rho})$. Estimation of the model parameters will now be considered.

3 Statistical modelling and estimation

As previously mentioned, EIT is an ill-posed inverse problem which will require regularisation to make stable estimation possible. This further modelling is most naturally discussed with the Bayesian modelling framework. In this approach the likelihood function above is combined with a prior distribution which quantifies expert opinion on the nature of the unknown quantities.

If we assume that there is no knowledge about the likely resistivity values but that they are expected to vary reasonable smoothly, then this suggests a Markov random field model, such as a Gaussian Markov model, which is written in terms of local variability. For example

$$\pi(\boldsymbol{\rho}) \propto \exp \left\{ -\frac{1}{2\tau^2} \sum (\rho_i - \bar{\rho}_i)^2 \right\} \quad (3.1)$$

where $\bar{\rho}_i$ is the mean of the neighbours of pixel i and the variance parameter, τ^2 , controls the amount of local smoothing. Although this is an improper prior, it will not create an improper posterior distribution. In the usual approach, where the contact impedances are assumed known, this is combined with the likelihood producing a posterior distribution

$$\pi(\boldsymbol{\rho}|\mathbf{V}, \mathbf{z}) \propto f(\mathbf{V}|\boldsymbol{\rho}, \mathbf{z})\pi(\boldsymbol{\rho}) \quad (3.2)$$

Estimates of $\boldsymbol{\rho}$ are now obtained as

$$\hat{\boldsymbol{\rho}} = \arg \max_{\boldsymbol{\rho}} \pi(\boldsymbol{\rho}|\mathbf{V}, \mathbf{z}). \quad (3.3)$$

In the approach proposed here, it is acknowledged that the contact impedances are not known, but must also be modelled and estimated. It will be assumed, however, that the prior information about \mathbf{z} is independent of that about $\boldsymbol{\rho}$ and hence the joint prior can be written as the product of two separate components, that is $\pi(\boldsymbol{\rho}, \mathbf{z}) = \pi(\boldsymbol{\rho}) \times \pi(\mathbf{z})$ where the prior distribution for the contact impedances be denoted, $\pi(\mathbf{z})$. Hence the posterior density, to be used for estimation is now

$$\pi(\boldsymbol{\rho}, \mathbf{z}|\mathbf{V}) \propto f(\mathbf{V}|\boldsymbol{\rho}, \mathbf{z})\pi(\boldsymbol{\rho})\pi(\mathbf{z}) \propto \pi(\boldsymbol{\rho}|\mathbf{V}, \mathbf{z})\pi(\mathbf{z}). \quad (3.4)$$

It will later be shown that an independence assumption is reasonable, and hence $\pi(\mathbf{z}) = \pi(z_1) \cdot \pi(z_2) \cdots \pi(z_K)$. Joint estimates of $\boldsymbol{\rho}$ and \mathbf{z} would then be given by

$$(\hat{\boldsymbol{\rho}}, \hat{\mathbf{z}}) = \arg \max_{\boldsymbol{\rho}, \mathbf{z}} \pi(\boldsymbol{\rho}, \mathbf{z}|\mathbf{V}). \quad (3.5)$$

In practice the contact impedances are nuisance parameters, and hence estimation is performed using the marginal posterior density

$$\pi(\boldsymbol{\rho}|\mathbf{V}) = \int_{\mathbf{z}} \pi(\boldsymbol{\rho}, \mathbf{z}|\mathbf{V}) d\mathbf{z} \propto \int_{\mathbf{z}} \pi(\boldsymbol{\rho}|\mathbf{V}, \mathbf{z}) \pi(\mathbf{z}) d\mathbf{z} \quad (3.6)$$

then

$$\hat{\boldsymbol{\rho}} = \arg \max_{\boldsymbol{\rho}} \pi(\boldsymbol{\rho}|\mathbf{V}). \quad (3.7)$$

This estimate can be approximated, using an importance sampling approach, as

$$\hat{\boldsymbol{\rho}} = \frac{1}{M} \sum_{i=1}^M \boldsymbol{\rho}_i^* \quad (3.8)$$

where $\boldsymbol{\rho}_i^*$ is the posterior estimate of $\boldsymbol{\rho}$ calculated using a set of contact impedance values \mathbf{z}_i , that is

$$\boldsymbol{\rho}_i^* = \arg \max_{\boldsymbol{\rho}} \pi(\boldsymbol{\rho}|\mathbf{V}, \mathbf{z}_i), \quad i = 1, 2, \dots, M, \quad (3.9)$$

where \mathbf{z}_i is a set of contact impedances drawn from the prior distribution, that is $\mathbf{z}_i \sim \pi(\mathbf{z})$, and using the independence assumption, $z_{i,1} \sim \pi(z_1)$, $z_{i,2} \sim \pi(z_2) \dots z_{i,K} \sim \pi(z_K)$, with $\mathbf{z}_i = (z_{i,1}, z_{i,2}, \dots, z_{i,K})$. An initial calibration stage of the experiment will be used to estimate the separate contact impedance prior distributions, and also to validate the independence assumption.

4 Experimental results from EIT data

4.1 Data description

A sequence of nine laboratory experiments were undertaken to investigate the mixing of two liquids in a tank. The circular cross-sectioned tank had a diameter of 15cm and a height of 30cm, with eight electrodes of height 3cm and width 1cm, extending the whole depth of the liquid contents. At the start of the experiments the tank contained plain water. Then, occasionally, the water was stirred and at four well-spaced times concentrated potassium chloride solution was injected into the tank. During some of the other experiments solid objects were placed into the tank but these are not important for the current paper. Further details of the experimental set-up can be found in (West, Meng, Aykroyd and Williams, 2005).

In one of the experiments, after an initial stationary period, the water was stirred and then left for about 100 time points. This creates the first dataset analysed to investigate temporal stability of the contact impedance values, and will be referred to as the *temporal* data. Further, it is important to note that each of the nine experiments started with the tank containing a homogeneous internal resistivity distribution with data recorded at between 5 and 10 time points at approximately 2 second intervals. In the original experimental design it was intended that data

from these time points would be used for calibration – this part of each experiment is referred to as *calibration data*. Also, in four of these experiments concentrated potassium chloride solution was injected into the tank. Hence, this creates the second set of data to be analysed made-up of nine calibration datasets to allow the study of the influence of changes in internal resistivity on the electrode contact impedances. The first three expected to have constant internal resistivity, the next four have successive reductions in resistivity, with the final two fixed at the lowest resistivity level.

4.2 Analysis of calibration data

The calibration data contains 100 data points, referred to as frames, each with 49 measured voltages. Figure 1 shows scatterplots for the estimates of resistivity, $\hat{\rho}$, and the eight contact impedances, $\hat{z}_1, \hat{z}_2, \dots, \hat{z}_8$, for the 100 frames. In all panels there is substantial variation but no apparent systematic pattern, such as serial correlation.

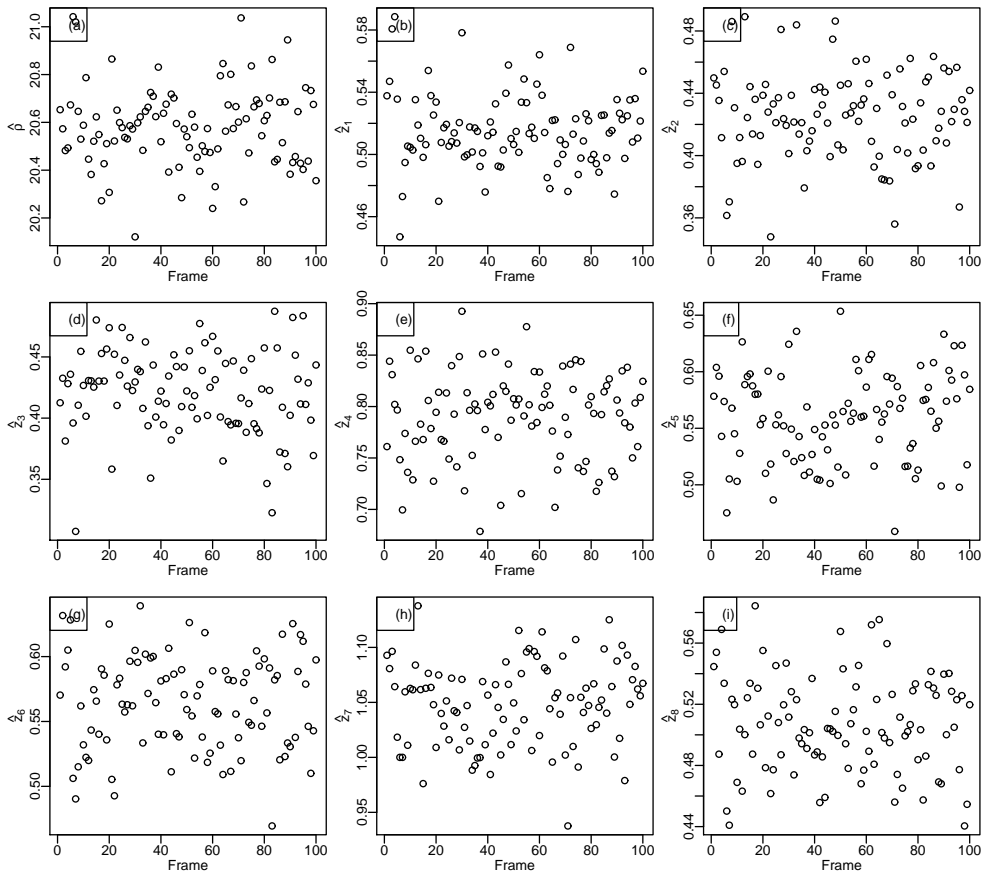


Figure 1: Scatterplots of estimated resistivity and electrode contact impedances.

Figure 2 shows the same information as a kernel density estimate (in grey), using R function `density` with default settings, along with fitted Gaussian curves (in black). Corresponding sample mean, standard deviations, skewness and kurtosis are shown in Table 1. Figures 3 sum-

marises the values as boxplots. The resistivity estimates are centred on $20.6 \Omega m$ with moderate standard deviation showing good stability within the temporal sequence. The electrode contact impedances are also consistently estimated with slightly narrower distribution for \hat{z}_1 , the contact impedance for the reference electrode, than the other electrodes. There have, however, very different values ranging from mean values of 0.42 to 1.05. The skewness and excess kurtosis values, along with the density and boxplots, indicate good agreement with a Gaussian distribution. Applying the Shapiro-Wilk normality test accepts normality (applying the Bonferroni correction turns the one marginally significant value leading to all clearly non-significant). The autocorrelation functions, shown in Figure 4, contain a few values marginally outside the confidence bands. None of these are substantial and hence supports an absence of temporal correlation. This indicates that the separate frames in the sequence can be treated as independent.

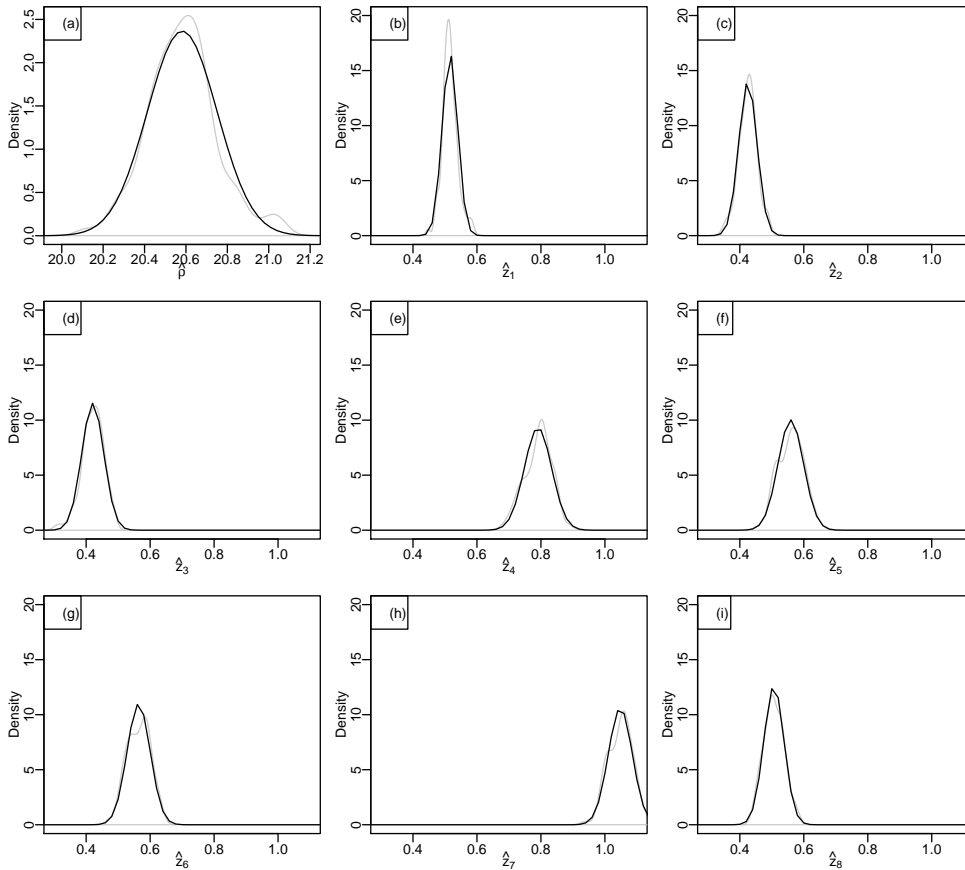


Figure 2: Kernel density estimates (in grey) and fitted Gaussian curves (in black) of the estimated resistivity and electrode contact impedances.

4.3 Estimation of resistivity

In this section the frames from the nine calibration phases are analysed estimating interior resistivity, ρ , and electrode contact impedances, z_1, z_2, \dots, z_8 . Recall that during each of experiments

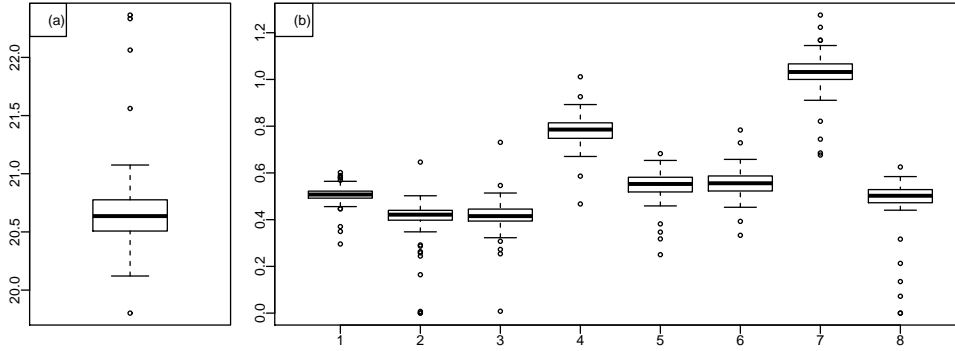


Figure 3: Boxplots of the estimates of resistivity and electrode contact impedances.

	Mean	Std. Dev.	Skewness	Kurtosis
ρ	20.5822	0.1687	0.2635	0.5507
z_1	0.5156	0.0241	0.4442	0.9191
z_2	0.4252	0.0285	-0.1655	0.1204
z_3	0.4207	0.0346	-0.5481	0.5075
z_4	0.7908	0.0428	-0.3096	-0.3550
z_5	0.5594	0.0398	-0.0817	-0.5974
z_6	0.5640	0.0363	-0.1331	-0.6724
z_7	1.0482	0.0376	-0.1732	-0.3202
z_8	0.5066	0.0316	0.1295	-0.4715

Table 1: Summary results of estimation across $n = 100$ real datasets showing mean, standard deviation, skewness and kurtosis for the resistivity (Ωm) and contact impedance (Ω) estimates.

3 to 6, concentrated potassium chloride solution was injected into tank of water. Before the next set of calibration frames this will have completely dispersed producing another homogeneous internal resistivity distribution, but with a lower resistivity.

Figure 5 shows the sequence of estimated resistivity and contact impedance values. The dots show the mean value of five frames surrounded by a grey region indicating the range of values with the five estimates. The black dots represent estimates from datasets immediately following the addition of salty water, whereas the black dots come from datasets following no change. In (a) the estimated resistivity values start just above $20\Omega m$ for the first three experiments. After the first injection of salty water the next estimate of resistivity jumped down to about $5\Omega m$. The subsequent estimates show a further gentle reduction in value. The grey band is very narrow for the six cases but increases moderately for the final three values. These resistivity estimates in agreement with recognised values (Helmenstine, 2016) of $20\Omega m$ (range 20-2000) for drinking water and $0.2\Omega m$ for salty (sea) water. The pattern is similar for the electrode contact impedances, in that there is initial high contact impedances, then a substantial decrease, and

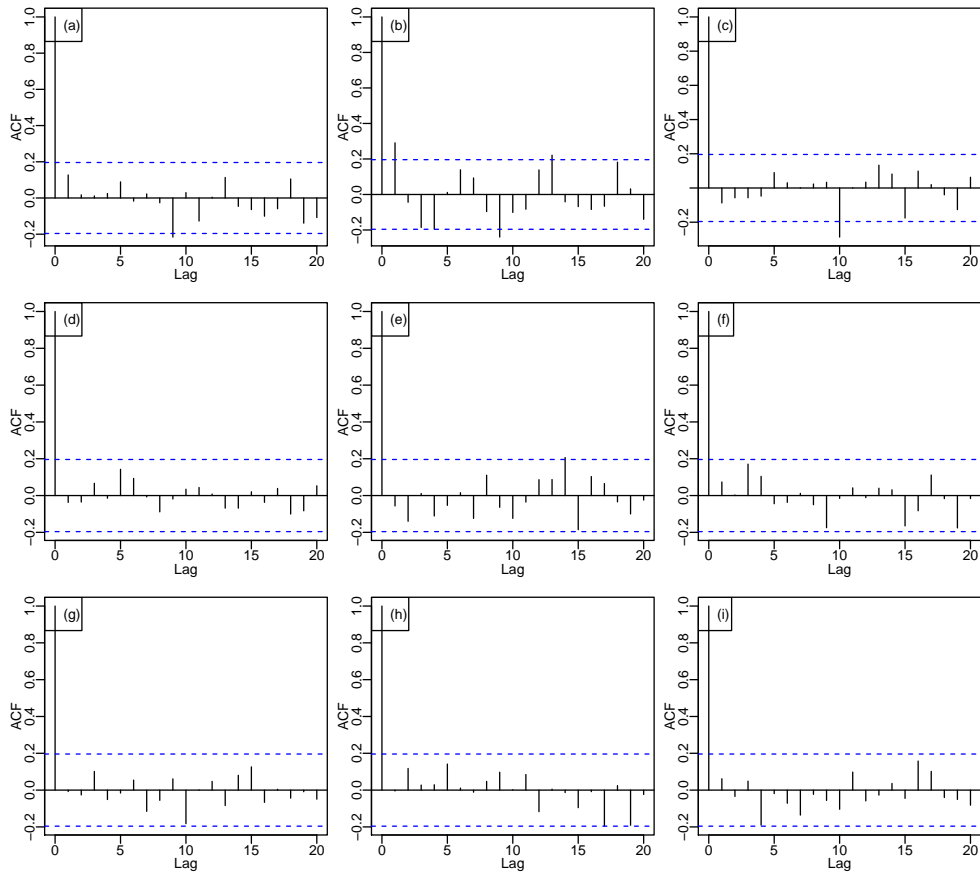


Figure 4: Autocorrelation functions for the estimates of resistivity and electrode contact impedance.

finally a small increase. There is also a final increase in the range of estimates, especially in the final three of four cases. These results show that there is substantial differences between the electrode contact impedances, varying from about 0.4 to more than 1.0Ω . Further, the values vary substantially across the nine experiments and suggest that great care must be used when setting contact impedances for estimates of an internal inhomogeneous resistivity distribution.

4.4 Reconstruction of resistivity distributions

In this section previous results are used in the reconstruction of an internal inhomogeneous resistivity distribution. The third experiment was the first which included the addition of concentrated potassium chloride.

The calibration frames, time points 1 to 5, are combined with the final five frames, time points 44 to 49, are combined and analysed as in the previous section with their mean, standard deviation and range shown in Table 2. Although the mean values might give a *typical* value, there is

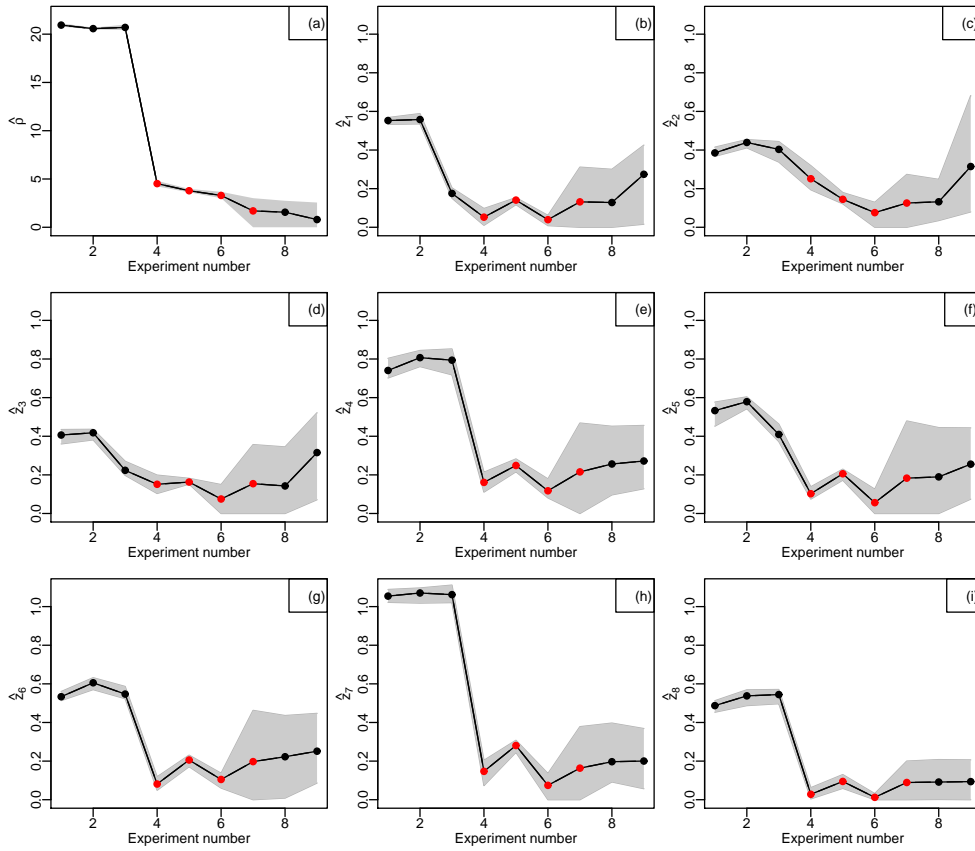


Figure 5: Model estimates (points and line with range shown as a grey band) from sequence of experiments, where the red points correspond to experiments including addition of salty water.

substantial variation. Fixing values at the mean might give a potentially misleading interpretation from any resulting reconstruction.

Figure 6 shows a standard reconstruction using the mean contact impedance values given in Table 2. The low resistivity region in the top-left is clearly visible indicating the location of the added salty water. There is a reasonably constant background resistivity, about $20\Omega m$, and a well-defined low resistivity region, of about $5\Omega m$.

Using the approach proposed early, 100 sets of electrode contact impedances are simulated from independent Gaussian distributions using the means and standard deviations in Table 2. This results in 100 estimates of the internal resistivity distributions. These have been summaries by their mean and width of a confidence interval in Figure 7. The model average is very similar to the single reconstruction with fixed contact impedances shown on Figure 6, but the confidence interval width image shows substantial and spatially correlated values. These latter values can be as large as $4\Omega m$ which represents a substantial extra contribution to the level of uncertainty. As a final comparison, Figure 8 shows the difference between the two mean value reconstructions in Figures 6 and 7(a). The differences range from almost -2 to $+1.5\Omega m$. These differences

	ρ	z_1	z_2	z_3	z_4	z_5	z_6	z_7	z_8
Mean	20.3145	0.2162	0.4321	0.2620	0.7882	0.4390	0.6017	1.0906	0.5688
Std. Dev.	0.8079	0.0796	0.0779	0.0718	0.0725	0.0607	0.0753	0.0704	0.0506
Min	18.1400	0.1507	0.3379	0.1978	0.6228	0.3725	0.5235	1.0208	0.4971
Max	20.9820	0.4274	0.6343	0.4398	0.8707	0.5382	0.7658	1.2662	0.6946

Table 2: Calibration results taken from Frames 1-10 showing mean and standard deviation for the resistivity (Ωm) and contact impedance (Ω) estimates.

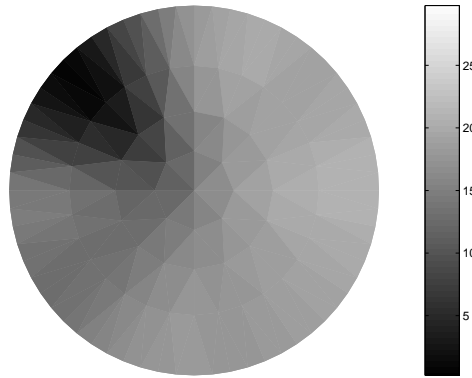


Figure 6: Standard Gauss-Newton reconstruction of resistivity distribution (Ωm).

being caused by variability in electrode contact impedances.

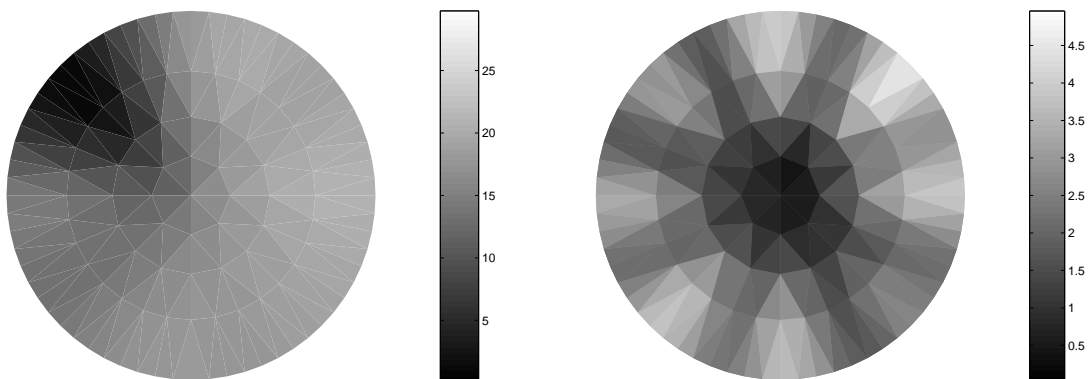


Figure 7: Result of model averaging (left) and corresponding width of confidence interval (right) – both expressing in Ωm .

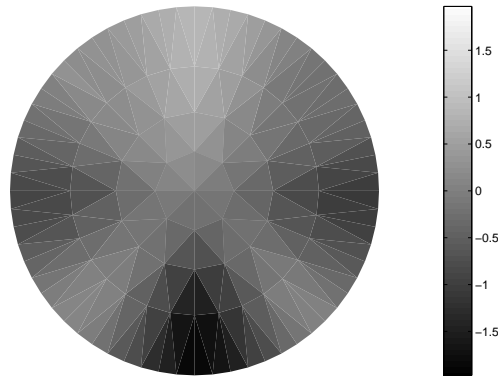


Figure 8: Residuals (Ωm).

5 Discussion

Electrical impedance tomography has the capability of providing unrivalled information about important processes. The technique is most widely used in industrial process monitoring where being non-invasive and being cheap make it ideal for visualizing otherwise inaccessible equipment. Of course, to obtain useful output from the image reconstruction requires accurate input. Although, the external voltage measurements provide the biggest component of the required input, electrode contact impedances make a vital contribution also. Although the contact impedance values from the calibration data should provide good estimates it is common for contact impedances to vary with time. This will be particularly true when changes in internal resistivity are also present. The results presented here have demonstrated this using real experimental data. It is impossible that the contact impedances are known, and standard values from previous research is likely to be of little value. It is necessary to assign individual values for different electrodes and to incorporate uncertainty into the reconstruction process.

A simple approach has been proposed to incorporate this extra source of variability into the estimation of the internal resistivity distribution. The fitted distributions for the contact impedances from calibration data are used to simulate a sample of possible sets of contact impedance, and each of these is then used in the reconstruction algorithm. A final reconstruction is produced by averaging, and the usual measures of reliability and reproducibility can be obtained by combining those from the sample of reconstructions. For example the total variance would be calculated as the mean of the variances from the separate reconstructions plus the variance between the separate reconstructions—a sum of within-group and between-group variability.

Whenever estimation and reconstruction are performed it is vital that care is taken to correctly quantify uncertainty. It is hoped that this work has highlighted the need for further modelling. This means identifying and measuring variability from different sources. Only with careful modelling and calculation can results be used reliably. Such consideration can have great impact on the

decision making.

Acknowledgements The real mixing data were collected while the author, and others, were supported by the EPSRC through grant GR/R22148/01. Also, during the early stages of this research the author was taking part in a Visiting Fellowship programme supported by the University of Technology Sydney, Australia. The author acknowledges, and is grateful to, both of these organisation. The author is also grateful to Chris Oates whose casual comment one day provided the motivation for this work.

References

- Heikkinen, L. M., Vilhunen, T., West, R. M. and Vauhkonen, M. 2002. Simultaneous reconstruction of electrode contact impedances and internal electrical properties: II. Laboratory experiments, *Meas. Sci. Technol.* **13**: 1855–1861.
- Helmenstine, A. M. 2016. Table of resistivity and conductivity at 20c, [urlhttp://chemistry.about.com/od/moleculescompounds/a/Table-Of-Electrical-Resistivity-And-Conductivity.htm](http://chemistry.about.com/od/moleculescompounds/a/Table-Of-Electrical-Resistivity-And-Conductivity.htm). Accessed: 2016-11-30.
- Kaipio, J., Kolehmainen, V., Vauhkonen, M. and Somersalo, E. 1999. Inverse problems with structural prior information, *Inverse Problems* **15**: 713–729.
- Lionheart, W. R. 2004. EIT reconstruction algorithms: Pitfalls, challenges and recent developments, *Physiological Measurement* **25**: 125–142.
- Paulson, K., Breckon, W. and Pidcock, M. 1992. Electrode modelling in electrical impedance tomography, *SIAM J. APPL. MATH.* **52**: 1012–1022.
- Polydorides, N. and Lionheart, W. R. B. 2002. A Matlab toolkit for three-dimensional electrical impedance tomography: a contribution to the electrical impedance and diffuse optical reconstruction software project, *Meas. Sci. Technol.* **13**: 1871.
- Somersalo, E., Cheney, M. and Isaacson, D. 1992. Existence and uniqueness for electrode models for electric current computed tomography, *SIAM J. Appl. Math.* **52**: 1023–1040.
- Vauhkonen, M., Lionheart, W. R. B., Heikkinen, L. M., Vauhkonen, P. J. and Kaipio, J. P. 2001. A MATLAB package for the EIDORS project to reconstruct two-dimensional EIT images, *Physiological Measurements* **22**: 107–111.
- Vilhunen, T., Kaipio, J. P., Vauhkonen, P. J., Savolainen, T. and Vauhkonen, M. 2002. Simultaneous reconstruction of electrode contact impedances and internal electrical properties: I. Theory, *Meas. Sci. Technol.* **13**: 1848–1854.

West, R., Meng, S., Aykroyd, R. and Williams, R. 2005. Spatial-temporal modeling for electrical impedance imaging of a mixing process, *Review of Scientific Instruments* **76**: 073703–073703–10.